

Review: Prediction of Unexpected Fluid-Induced Vibration in Pipeline Network

Ryuhei Yamaguchi*, Makoto Ohta

Institute of Fluid Science, Tohoku University, Sendai, Japan

Email: *ryuhei63@gmail.com

How to cite this paper: Yamaguchi, R. and Ohta, M. (2022) Review: Prediction of Unexpected Fluid-Induced Vibration in Pipeline Network. *World Journal of Mechanics*, 12, 17-40.

<https://doi.org/10.4236/wjm.2022.122002>

Received: January 12, 2022

Accepted: February 25, 2022

Published: February 28, 2022

Copyright © 2022 by author(s) and Scientific Research Publishing Inc.

This work is licensed under the Creative Commons Attribution-NonCommercial International License (CC BY-NC 4.0).

<http://creativecommons.org/licenses/by-nc/4.0/>



Open Access

Abstract

This review considers unexpected destructive disasters involving fluid power plants, such as nuclear electric power plants and fluid power plants. It specifically addresses the possibility of fluid vibration induced in a pipeline network of such a plant. The authors investigate the flow oscillation induced within a T-junction for laminar steady flow at a Reynolds number less than 10^3 and clarify that there is a periodic fluid oscillation with a constant Strouhal number independent of several flow conditions. Generally, a nuclear electric power plant is constructed using straight pipes, elbows, and T-junctions. Indeed, a T-Junction is a basic fluid element of a pipeline network. The flow in a fluid power plant is turbulent. There are peculiar flow phenomena that occur at high Reynolds numbers, which are also seen in other flow situations; e.g., Kaman vortices are observed around a circular cylinder in low Reynolds numbers, around structures like bridges and downstream of islands in oceans. Although the flow situation of a T-junction and elbow in a fluid power plant, such as the fluid suddenly changing its flow direction is turbulent flow, the authors mention the possibility of the fluid-induced vibration of a pipeline network.

Keywords

Fluid-Induced Vibration, Flow Oscillation, Tube Flow, Laminar Steady Flow, Fluid Power Plant

1. Introduction

The Karman vortex was first reported by von Kármán (1911, 1912) [1] [2] and Benard (1908) [3] and. The collapse of a bridge spanning the Takoma Narrows (1940) was a typical destructive incident resulting from a Karman vortex [4]. Meanwhile, a thermocouple in the Monju fast breeder reactor was destroyed by

fluid-induced vibration and a fine tube fractured in the steam evaporator of the second unit of the Mihama Nuclear Power Plant [5] [6].

There have been destructive accidents in which fluids have induced the vibration of engineering structures, such as bridges, pipeline networks, and fluid power plants [1] [2]. It is difficult for the engineer and designer to predict such unexpected destructive phenomena related to fluid vibration. There might be a few possibilities of unpredictable fluid-induced vibration.

Brown & Roshko [7], Tani [8], and Taneda [9] clarified that a high shear rate induces flow instability. Oscillation, self-sustaining oscillation, and flow instability have been studied experimentally for a cavity flow [10] [11] and flow through an axisymmetric stenosed channel [12]. Mori & Naganuma [13] clarified the coherent oscillation of incompressible turbulent flow over a rectangular cavity experimentally. Flow instability has also been observed in a nasal channel and for a cantilevered flexible plate [14] [15] [16]. However, this flow instability can appear as weak periodic oscillations rather than strong periodic oscillations. The vibration of turbulent fluid passing through an elbow has been analyzed by Keshtkar & Jafari numerically [17]. Researchers in the field of hemodynamics have extensively investigated flow instability induced inside cerebral aneurysms in terms of the growth and rupture of the aneurysms [18]-[23]. Indeed, although there is flow instability and turbulence within a cerebral aneurysm which the flow instability affects the rupture of an aneurysm.

Flow instability is a common interest in fluid mechanical engineering. There are several phenomena of unstable flow at the interface of two viscous fluids in a turbulent region. Awasthi *et al.* [24] investigated the Rayleigh-Taylor instability of two viscous fluids enclosed by two cylindrical coaxial surfaces considering mass and heat transfer across the interface. The Richtmyer-Meshkov instability has been investigated in numerical and experimental studies. Bernard *et al.* [25] experimentally investigated the primary features of flow developing after a shock acceleration and found that a well-studied method of flow visualization did not produce a flow pattern that matched the numerical model. Liu & Lu [26] investigated the flow instability of viscoelastic annular liquid jets in a radial electric field and found that the jets with reasonable parameters had greater instability. Bouzgarrou [27] investigated the development of a turbulent mixing zone induced by the Richtmyer-Meshkov instability and its subsequent evolution.

This review focuses on several phenomena of the destructive potential of fluid-induced vibration in the pipeline network of a fluid power plant.

2. Examples of Karman Vortex

Five examples of flow instability in internal and external flow are described.

2.1. Karman Vortices on Medium and Large Scales

The most aesthetically attractive phenomenon of flow instability in the field of fluid dynamics is the Karman vortex at a Reynolds number less than approximately 100 as shown in **Figure 1** [9]. This vortex is generated by high-shear-rate



Figure 1. Karman vortex downstream of circular cylinder.

flow associated with the Kelvin-Helmholtz instability. The destructive collapse of a bridge spanning the Takoma Narrows Bridge, as shown in **Figure 2**, was directly related to this phenomenon [14]. As an example of the phenomenon at a large scale, Karman vortices appear around islands in the ocean, as shown in **Figure 3(a)** and **Figure 4**. The scale of Jeju Island and wind direction are shown in **Figure 3(b)** [28]. The Reynolds number is calculated to be on the order of 10^{11} from a characteristic distance $L = 30$ km along the wind direction, an assumed wind velocity $U = 50$ m/s at an altitude of 5000 m, and a molecular kinematic viscosity $\nu_{mole} = 2.47 \times 10^{-5}$ m²/s (-23°C):

$$Re = UL/\nu_{mole} = 50 \times 30 \times 10^3 / 2.47 \times 10^{-5} = 0.60 \times 10^{11}.$$

This Reynolds number is extremely large in comparison with that of a circular cylinder. Generally, the eddy kinematic viscosity or turbulent kinematic viscosity ε_{eddy} is adopted in the meteorological field for huge-scale flow:

$$\tau_{xy} = \rho [u'v'] = \rho \varepsilon_{eddy} (dU/dy),$$

where u' , v' , and ρ respectively denote the velocity fluctuations along the wind direction and perpendicular direction and the density at an altitude of 5000 m. When postulating to be $U = 50$ m/s and $v = 5$ m/s, the velocity fluctuation is assumed to be 10% and 20% of each velocity, velocity fluctuation will be $u' = 5$ m/s and $v' = 1$ m/s and density is $\rho = 0.648$ kg/m³. The eddy kinematic viscosity is thus obtained as $\varepsilon_{eddy} = \rho[u'v']/\rho(dU/dy) = 3.24 \text{ m}^2/[0.648 \text{ kg/m}^3(10 \text{ m/s}/10 \text{ m})] = 5 \text{ m}^2/\text{s}$. The Reynolds number for this stream is thus calculated as $Re = L(30 \text{ km}) \times U(50 \text{ m/s})/\varepsilon_{eddy}(5 \text{ m}^2/\text{s}) = 3 \times 10^5$. The order of 10^5 of this Reynolds number is comparable to those in the field of fluid engineering [29]

2.2. Flow Oscillation in a T-Junction

A T-junction at which a side-branch joins a trunk at a right angle is a fundamental fluid element of a pipeline network. In the past six decades, the pressure



Figure 2. Collapse of Takoma Narrows Bridge.

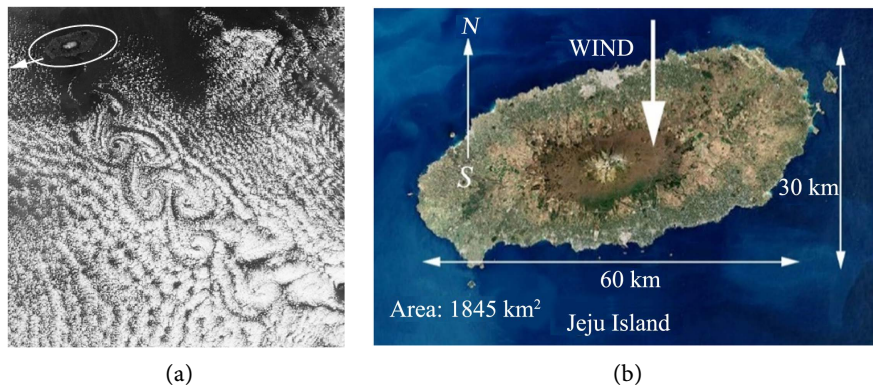


Figure 3. (a) Karman vortex downstream of Jeju Island; (b) Scale of Jeju Island.



Figure 4. Karman vortex around Canarias Islands.

loss through a T-junction has been extensively investigated and established for turbulent flow at a Reynolds number on the order of 10^5 in the field of engineering [29]. Furthermore, in the past four decades, the flow pattern and wall shear stress at a T-junction have been examined experimentally and numerically [30] [31] [32] for laminar steady flow in hemodynamics. Karino *et al.* investigated the flow pattern around a square-edged corner at the entrance of the side-branch of a T-junction using a microscope and showed how a helical flow in the side-branch results in recirculating flow [30]. Liepsch *et al.* [31] experimentally studied the flow structure within a T-junction for its relevance to hemodynamics. Using finite-volume and finite-element methods, Perktold *et al.* carried out three-dimensional calculations of the flow pattern in a branch for a bifurcation from the abdominal to renal artery [33]. Yamaguchi *et al.* [34] [35] [36] [37] [38] reported that a periodic oscillation generated in the side-branch of a T-junction at laminar steady flow of less than 10^3 . The Karman vortex and periodic oscillation in a T-junction are induced by similar flow instabilities.

2.3. Flow Instability in a T-Junction with Single Side-Branch

The present review focuses on fluid-induced vibration, primarily oscillation in a T-junction of a pipeline network, as shown in **Figure 5**. The inlet of the side-branch is a square-edged corner in the pipeline network of a fluid power plant. An open-end condition is applied at both outlets. The T-junction has a trunk radius $R_T = 12.2$ mm and side-branch radii $R_S = 4, 5, 7,$ and 9 mm (primarily, $R_S = 7$ mm). The flow division ratios Q_S/Q_T of the flow rate to the side-branch from the trunk are 0.25, 0.33, and 0.50 [39]. S_i denotes the measurement section.

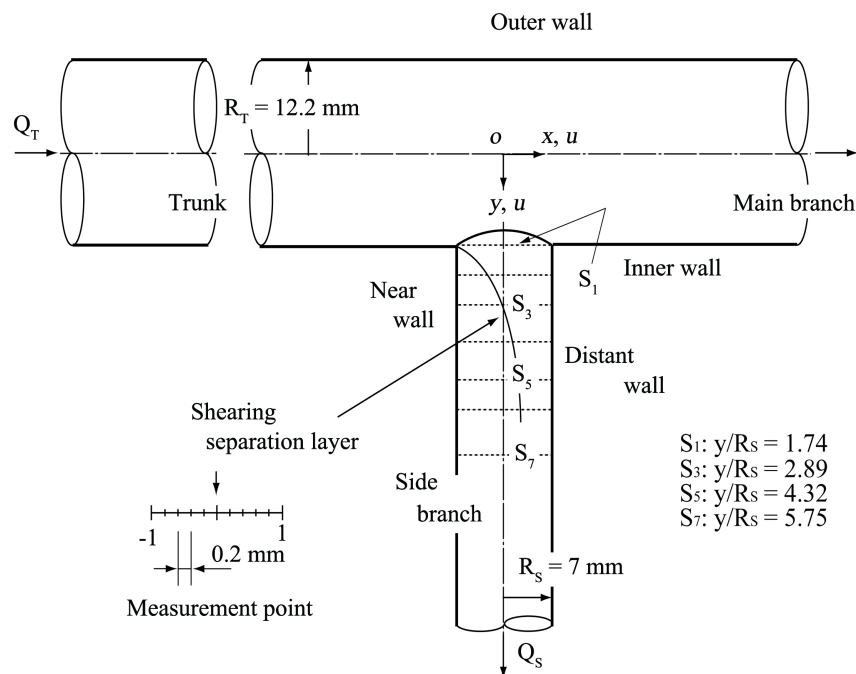


Figure 5. Schematic of T-junction and measurement sections S_i .

The kinematic viscosity of the working fluid (*i.e.*, the saturated aqueous iodide solution) is $\nu = 1.58 \times 10^{-6} \text{ m}^2/\text{s}$ [36]. The mean Reynolds numbers for the trunk and side-branch are primarily $Re_T = 800$ and $Re_s = 700$ ($Q_s/Q_T = 0.50$), respectively. **Figure 6** presents the results of particle image velocimetry (PIV) and laser Doppler velocimetry (LDV) [39]. Arrows depict velocity vectors and closed circles depict the locations of oscillation measurements spaced at intervals of 0.2 mm on the median plane of the side-branch. Along the near wall of the side-branch, the flow separates, reverses upstream, and with returns downstream along the shearing separation layer. The velocity along the near wall is low within the separation region and high outside the shearing separation layer as shown in **Figure 6**. There is thus a large velocity difference between two fluid flows across the shearing separation layer; *i.e.*, there is a high-shear-rate flow having an inflection point. This flow is strongly related to flow instability. **Figure 7** shows the profile of the tangential velocity q parallel to the shearing separation layer measured by PIV at points P_1 and P_2 with clear oscillation in both flow division ratios. At both flow division ratios, the inflection point across this shearing separation layer is clearly indicated. The shear rates $\Delta q/\Delta h$ at flow division ratios of $Q_s/Q_T = 0.25$ and 0.50 are 80 and 296 s^{-1} , respectively. These magnitudes of the shear rate in both flow division ratios are respectively three and six

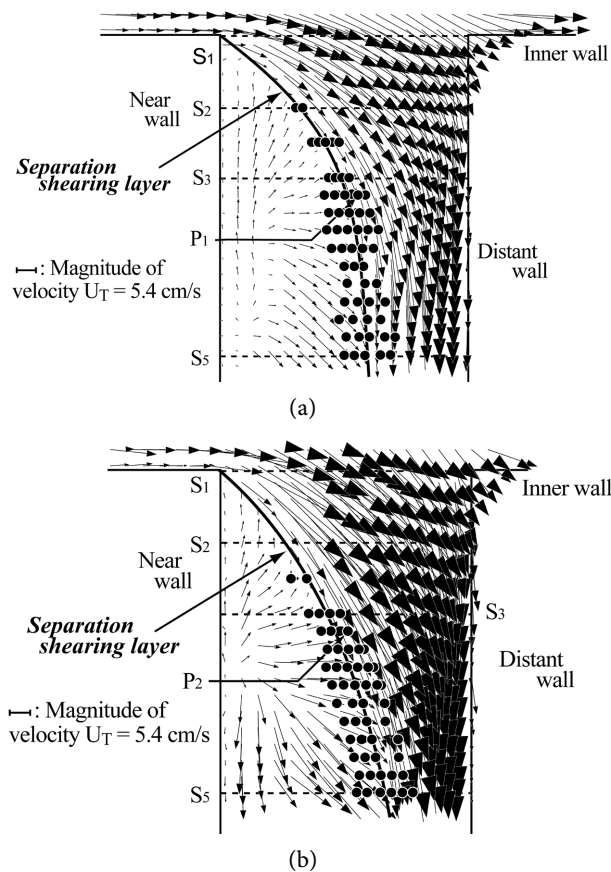


Figure 6. Velocity vector and oscillation point at median plane in side-branch. (a) $Q_s/Q_T = 0.25$; (b) $Q_s/Q_T = 0.50$.

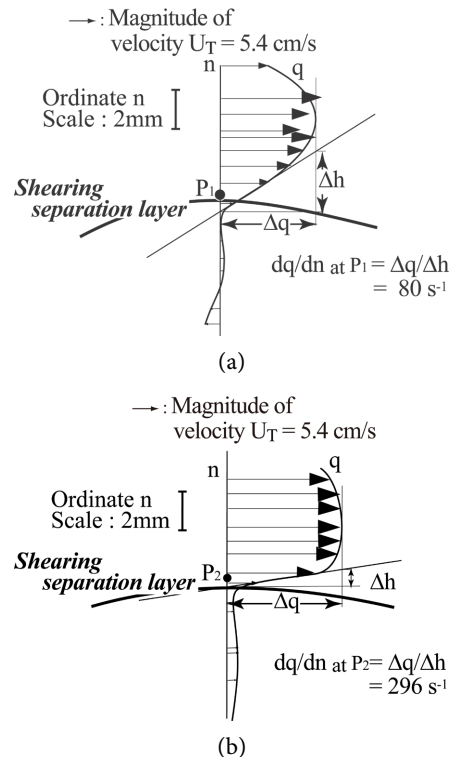
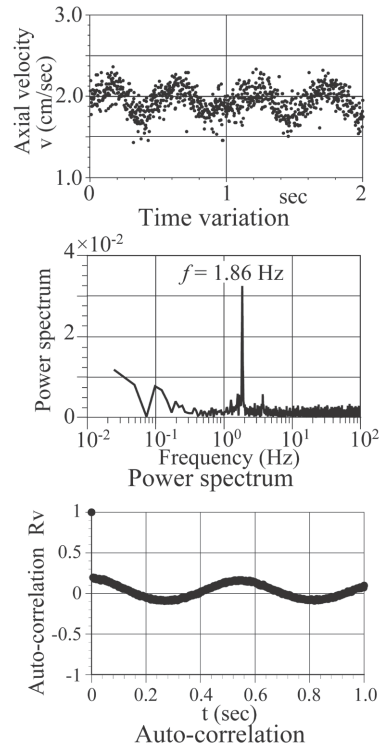


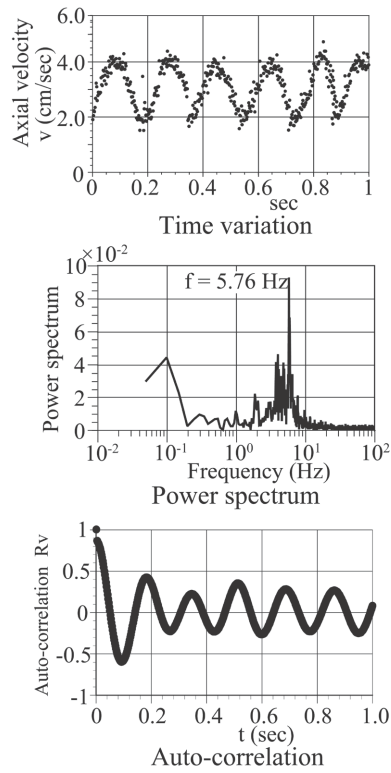
Figure 7. Tangential velocity profile along shearing separation layer. [(a) $Q_j/Q_T = 0.25$. (Shear rate downstream of side-branch = 24 s^{-1}), (b) $Q_j/Q_T = 0.50$. (Shear rate downstream of side-branch = 47 s^{-1})]

times those (24 and 47 s^{-1}) at the downstream wall of the side-branch. **Figure 8** presents the spectral analysis of the axial velocity at P_1 and P_2 measured by LDV to confirm the flow instability. The top, middle, and bottom panels respectively show the temporal variation of the axial velocity, power spectrum, and auto-correlation. In the T-junction, the frequencies of $f = 1.86$ and 5.76 Hz are respectively $Q_j/Q_T = 0.25$ and 0.50 in section S_3 . This frequency is the same value on the global median plane within the side-branch for each condition. Here, the diameter $D_s = 14 \text{ mm}$, the mean velocity $U_s = 0.08 \text{ m/s}$ at $Q_j/Q_T = 0.50$, and the Reynolds number Re_s and Strouhal number St_s of the side-branch are 700 and 1.01 respectively.

There is another source of flow instability in the T-junction. **Figure 9** presents the secondary velocity in three sections of the side-branch. In cross-section S_3 of the side-branch, the oscillation is strongly related to the high-shear-rate flow between two pairs of vortices with the same rotational sense in upper and lower half semi-circular sections. There is a small vortex at a lower left magnified circle in section S_3 for both flow division ratios. The mechanism underlying the fluid-induced oscillation is the high-shear-rate flow between two pairs of like-rotating vortices in section S_3 immediately downstream of the inlet of the side-branch. In particular, secondary flow immediately downstream of the upstream corner attracts the attention of the two pairs of vortices in the upper half circle at section S_3 ; *i.e.*, a small vortex appears at the near wall and a large vortex



(a)



(b)

Figure 8. Spectral analysis of axial velocity in side-branch at $Re_T = 800$. (a) $Q_J/Q_T = 0.25$ at point P_1 ($x/R_S = 0.09$, $y/R_S = 3.04$); (b) $Q_J/Q_T = 0.50$ at point P_2 ($x/R_S = -0.010$, $y/R_S = 3.04$).

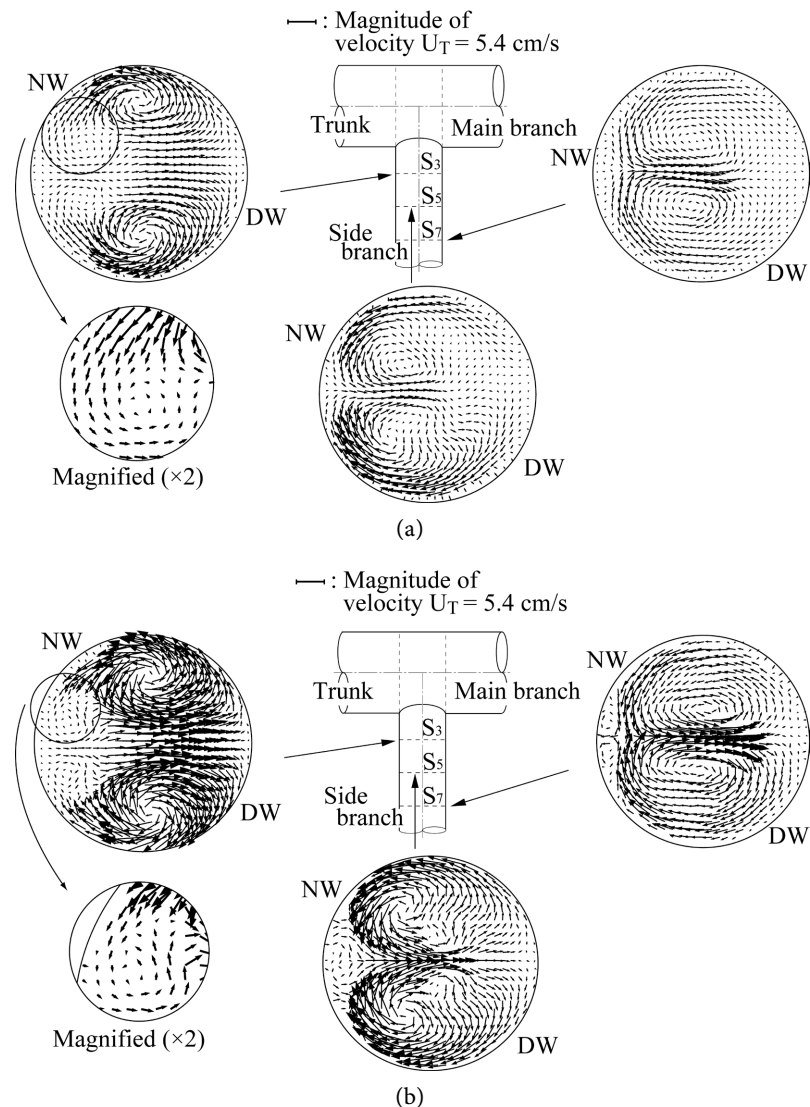


Figure 9. Secondary velocity at three cross sections in side-branch. (a) $Q_s/Q_T = 0.25$; (b) $Q_s/Q_T = 0.50$.

occupies the global median plane. Naturally, the two vortices have the same direction of rotational and there is thus friction between two vortices; *i.e.*, high-shear-rate induces flow instability. **Figure 10** shows the velocity profile of vortex and shear rate for two division ratios in section S_3 . There is a clear inflection in the velocity profile. The shear rates of 55 and 143 s^{-1} at the inflection point for flow division ratios of $Q_s/Q_T = 0.25$ and 0.50 are twice those (27 and 47 s^{-1}) for the downstream wall of the side-branch as shown in **Figure 10**, respectively.

There is a clear inflection in the velocity profile. The shear rates of 55 and 143 s^{-1} at the inflection point for flow division ratios of $Q_s/Q_T = 0.25$ and 0.50 are twice those (27 and 47 s^{-1}) for the downstream wall of the side-branch as shown in **Figure 10**, respectively. A periodic oscillation has been shown to be induced in the side-branch of a T-junction for steady laminar flow with Reynolds num-

ber in the above range (*i.e.*, $Re_s = 300$ to 900) [34] [35] [36] [39]. The Strouhal number of approximately 1.03 with a standard deviation of ± 0.26 based on quantities in the side-branch is regarded as independent of the Reynolds number, flow division ratio, and radius ratio of the side-branch to trunk as shown in **Figure 11** (open black symbols for a single side-branch). In the T-junction, the mean velocity U_s and the diameter D_s of the side-branch are considered characteristic quantities because the periodic oscillation appears in the side-branch. The characteristic flow behavior of the periodic oscillation in the side-branch is a universally recognized phenomenon of the T-junction [34] [35] [36] [39]. At $Re_T > 1000$ in the turbulent region, it is not possible to measure at a data rate much higher than the data rate of 3 kHz using the current LDV system (FSA-3500, TSI Co. LTD).

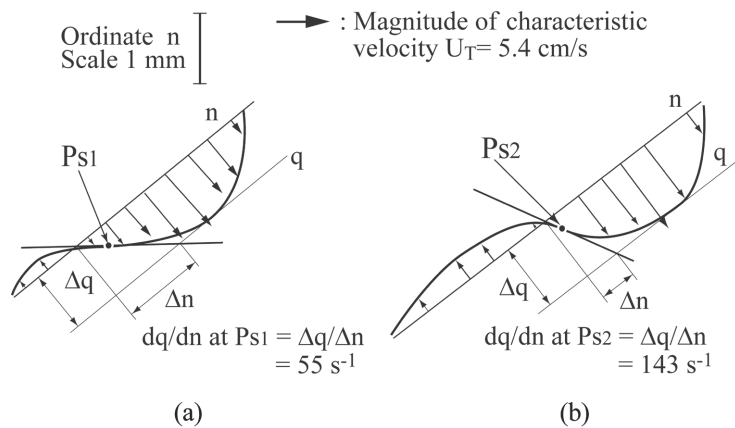


Figure 10. Secondary velocity and shear rate at boundary of two vortices in section S_3 . (a) $Q_s/Q_T = 0.25$; (b) $Q_s/Q_T = 0.50$.

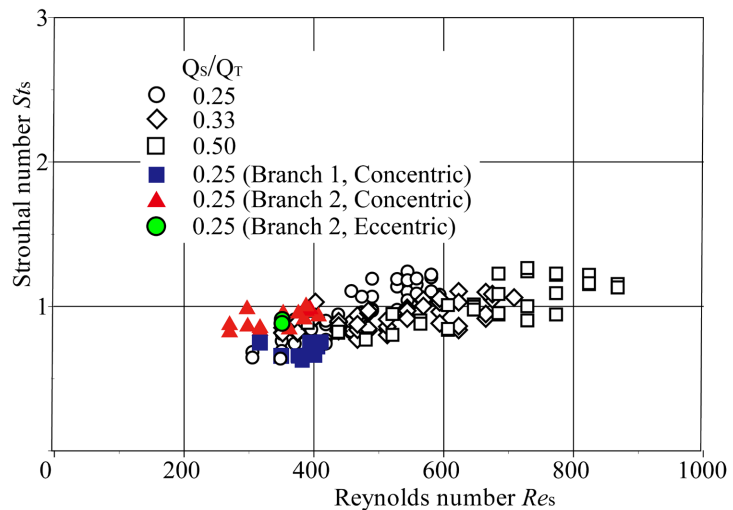


Figure 11. Side-branch Strouhal number St_s versus side-branch Reynolds number Re_s including double side-branches. ($Re_s = 2R_s U_s/\nu$ and $St_s = 2fR_s/U_s$. Open symbol is T-junction with single side-branch. \blacksquare and \blacktriangle denote concentric branch 1 and branch 2 in double side-branches, respectively. \bullet denotes eccentric branch 2) Mean value $(1.03) \pm$ S.D. (0.26) .

2.4. Flow Instability in a T-Junction with Two Side-Branches

This section describes the flow instability for two axis-aligned or axis-skewed open-ended side-branches of T-junctions. It also describes the mechanism of fluid-induced vibration in a T-junction with two side-branches bifurcating from a trunk in steady laminar flow for a single-phase [37]. **Figure 12(a)** shows the schema and labeling of the cross-section of axis-aligned side-branches in a T-junction with two concentric side-branches. **Figure 12(b)** shows a schema of the top and side views of the skewed branches of a T-junction with two eccentric side-branches. The center of the skewed side-branches has a radial offset of 1 and 2 mm at side-branches 1 and 2 in **Figure 12(b)** respectively, and the median planes in side-branches 1 and 2 are tilted away from that of the trunk axis.

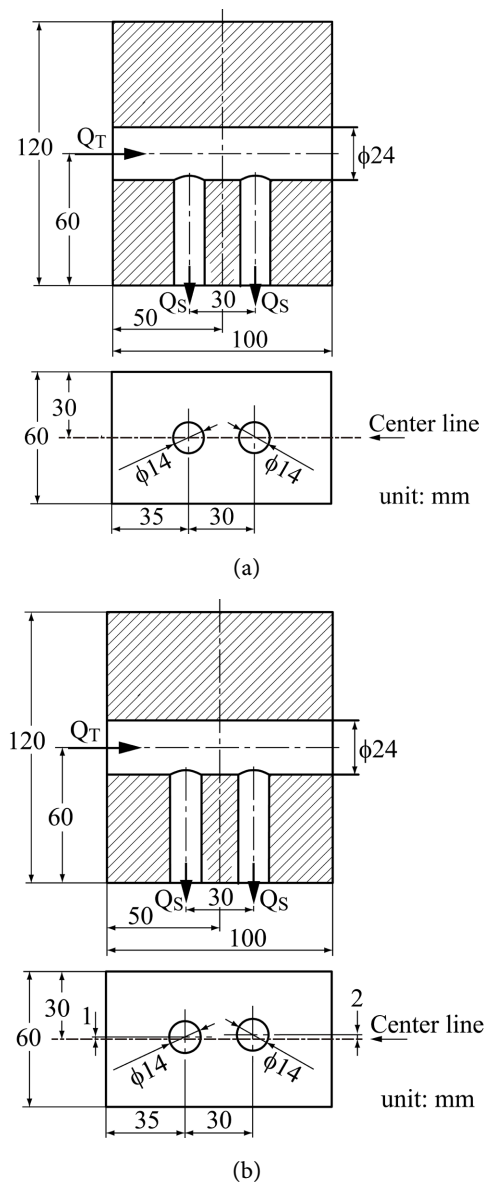


Figure 12. Schema of concentric and eccentric double side-branches in T-junction. (a) Concentric side-branch; (b) Eccentric side-branch.

The measurement method is the same as that used for the T-junction with the single side-branch described above except for the working fluid. The working fluid is 53% aqueous glycerin with a refractive index of 1.41, a density of $\rho = 1.13 \text{ g/cm}^3$, and a kinematic viscosity of $\nu = 7.00 \times 10^{-6} \text{ m}^2/\text{s}$ at 20°C . The measurement was primarily carried out at $Re_T = 2R_T U_T / \nu = 800$ for steady laminar flow in the trunk for both axis-aligned and axis-skewed T-junctions. The mean velocity in the trunk is $U_T = 23 \text{ cm/s}$. The flow division ratio Q_s/Q_T is set at 0.25 for both side-branches 1 and 2. A spacing of $L_s = 30 \text{ mm}$ between the two side-branches is set in the experiment. This is the minimum spacing for which extreme fluid interference between the side-branches is expected; the inner and outer diameters of the side-branch are 14 and 20 mm, respectively. In LDV, the velocity is measured with a data sampling resolution of $1 \mu\text{s}$ every 2 ms for a is set at 0.25 for both side-branches 1 and 2. A spacing of $L_s = 30 \text{ mm}$ between the two side-branches is set in the experiment. This is the minimum spacing for which extreme fluid interference between the side-branches is expected; the inner and outer diameters of the side-branch are 14 and 20 mm, respectively. In LDV, the velocity is measured with a period of 40 s, giving a 20-k data set.

The velocity vector, shearing separation layer, and points of periodic oscillation on the median plane of the concentric side-branch are shown in **Figure 13**. **Figure 14** presents the spectral analysis of the axial velocity at p_1 and p_2 in side-branches 1 and 2. The oscillation along the separation shearing layer in side-branch 2 appears clearer than that in side-branch 1 and has a frequency higher than that in side-branch 1.

Figure 15 presents the secondary flow in the three sections of the double-concentric side-branches 1 and 2. At least a pair of vortices appear in each section of both branches 1 and 2. **Figure 16** presents the vortex velocity and a clear inflection point in section S_3 along the near wall. In the vortex velocity at the boundary in section S_3 , the shear rate for side-branch 2 is 1.5 times that for the downstream side-branch. In the tangential velocity along with the separating shearing layer in section S_7 , the shear rate for side-branch 2 is 1.5 times that for the downstream side-branch as shown in **Figure 17**.

Velocity vectors on the median plane of the eccentric double side-branches of the T-junction are shown in **Figure 18**. The velocity vectors indicated by the red arrows show the flow with clear oscillation. The tangential velocity along the shearing separation layer in section S_5 is depicted in **Figure 19**. Across this layer, the velocity profile has an inflection point and the shear rate for side-branch 2 is twice that for the single side-branch. **Figure 20** and **Figure 21** respectively present the spectral analysis and auto-correlation for the data of side-branch 2.

Figure 11 presents the Strouhal number St_s versus Reynolds number Re_s for the concentric and eccentric double side-branches and the single side-branch. The Strouhal number of 1.03 based on quantities of the side-branch is independent of the Reynolds number ($Re_s = 230$ to 400), flow division ratio, and radius ratio of the side-branch to trunk for the two side-branches. This order of

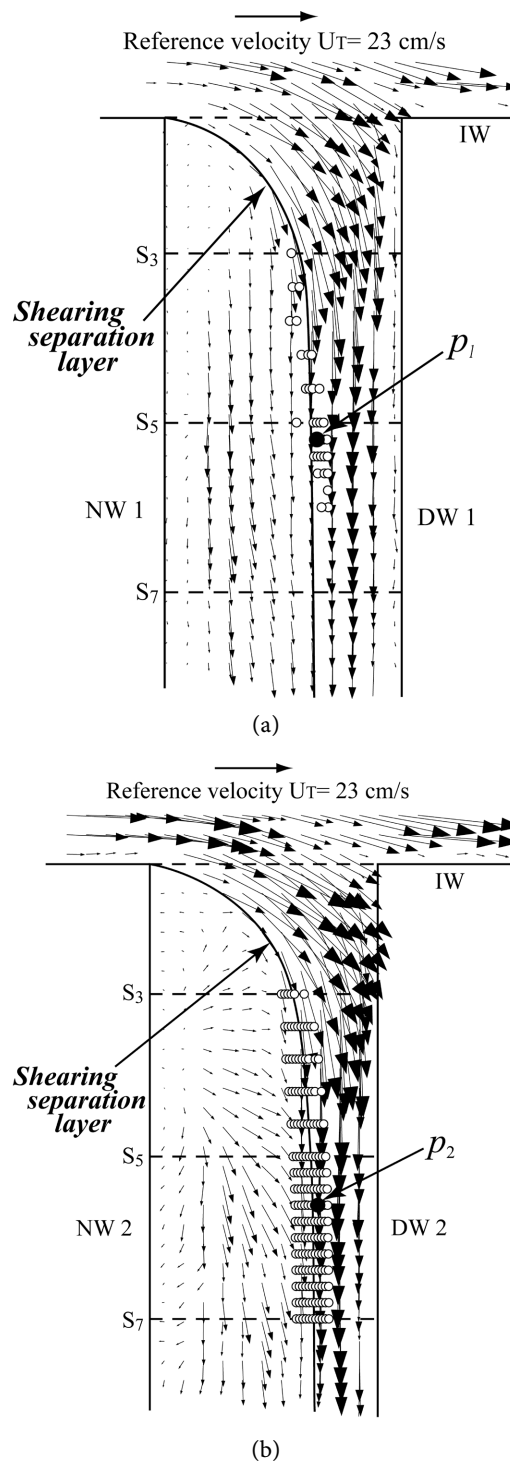
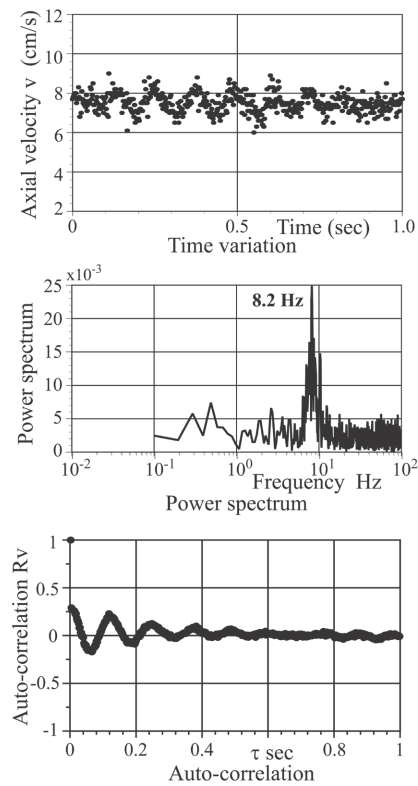
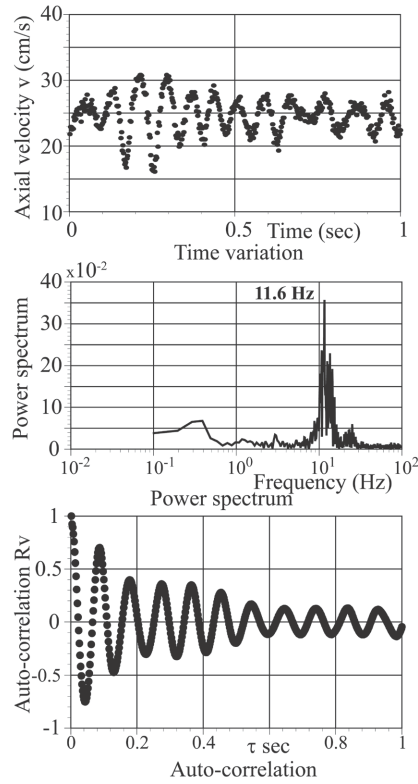


Figure 13. Velocity vector and oscillation point at median plane of concentric side-branch. (a) Side-branch 1 ($Q_{S1}/Q_T = 0.25$); (b) Side-branch 2 ($Q_{S2}/Q_T = 0.25$).

Reynolds number 10^5 is comparable to that in the field of fluid engineering. In other words, although the field of fluid engineering associates with the Karman vortex with molecular kinematic viscosity, the same feature is seen in meteorology.



(a)



(b)

Figure 14. Spectral analysis of axial velocity at p_1 near section S_5 in double concentric side-branches. (a) Side-branch 1 at p_1 ; (b) Side-branch 2 at p_2 .

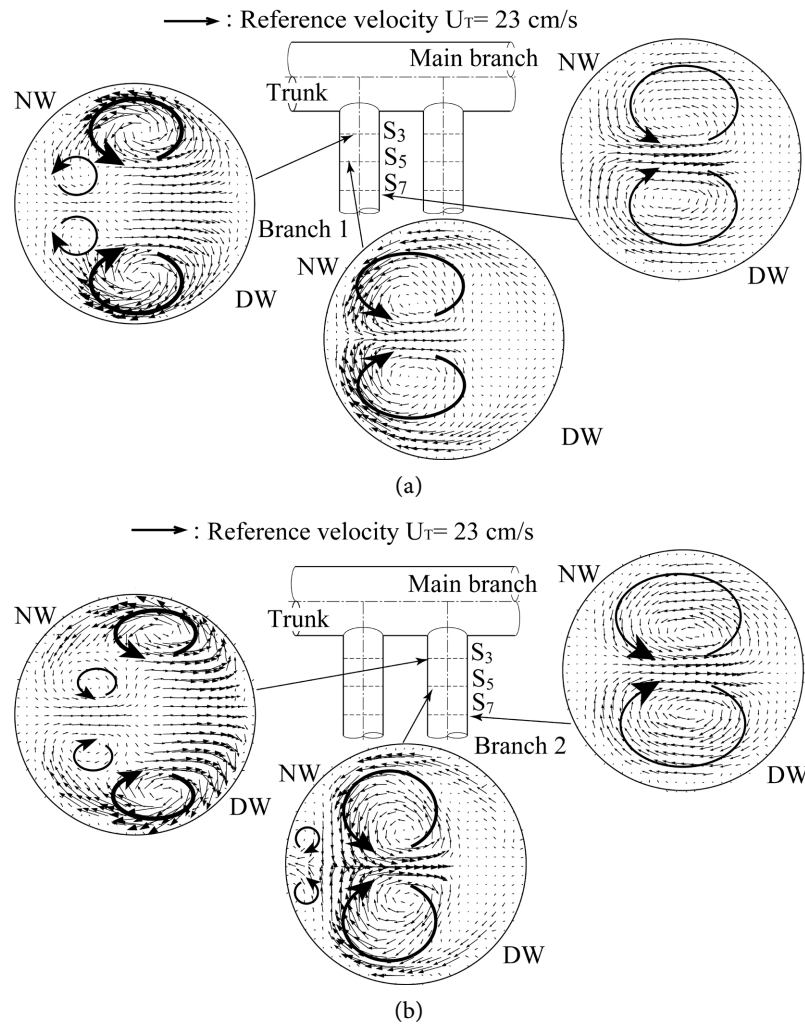


Figure 15. Secondary flow at three sections in double concentric side-branches. (a) Side-branch 1; (b) Side-branch 2.

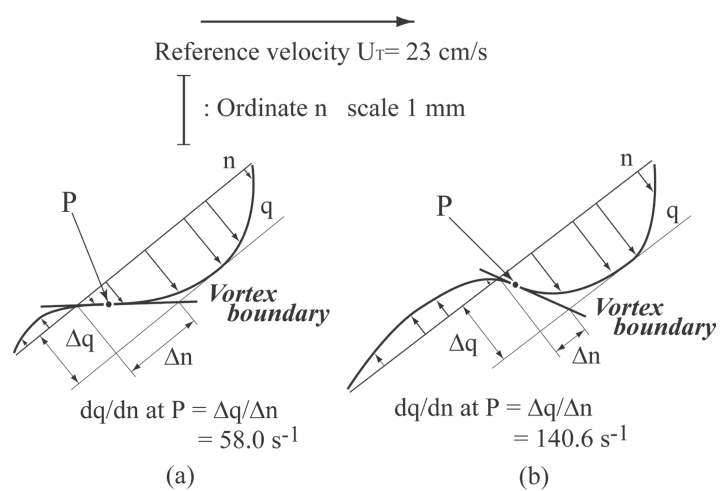


Figure 16. Inflection point and shear rate at vortex boundary near section S_3 in double concentric side-branches. [Velocity gradient $d\mathbf{v}/dx$ at wall ($x = R_3$) of side-branch = 96.6 s^{-1}]. (a) Side-branch 1; (b) Side-branch 2.

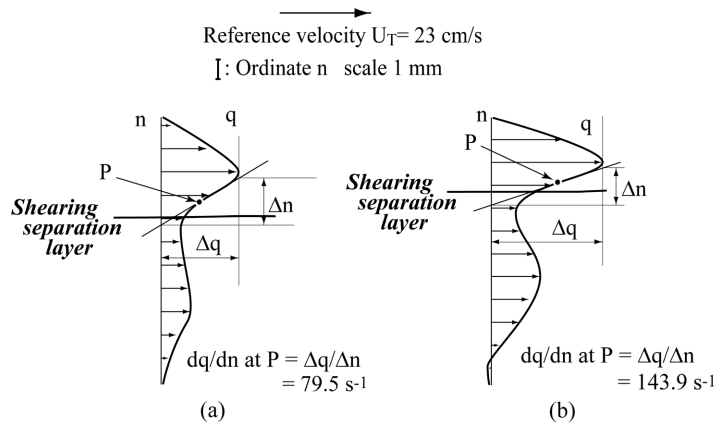


Figure 17. Tangential velocity profile along shearing separation layer with inflection point near section S_7 in double concentric side-branches. [Velocity gradient dV/dx at tube wall ($x = R_2$) of side-branch = 96.6 s^{-1}]. (a) Side-branch 1; (b) Side-branch 2.

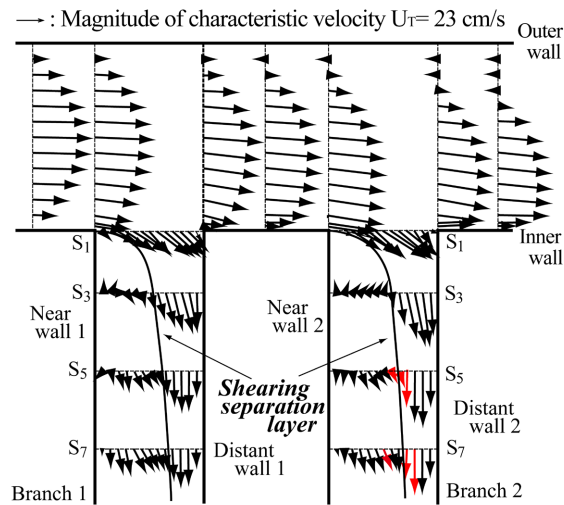


Figure 18. Velocity vector in eccentric side-branches in T-junction at median plane.

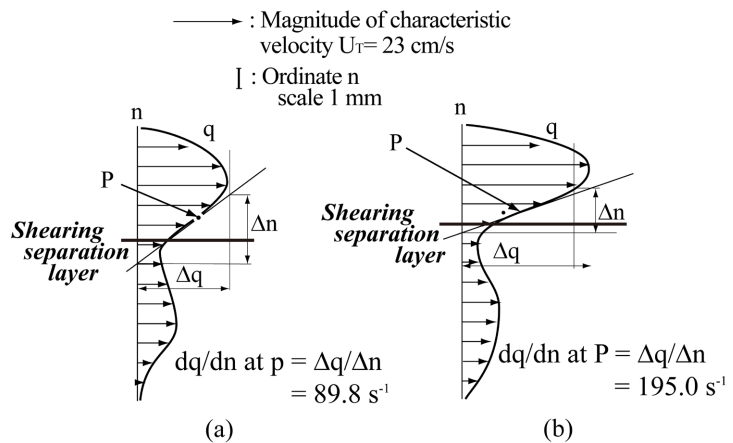


Figure 19. Tangential velocity profile along shearing separation layer with inflection point near section at section S_5 in eccentric side-branches [Velocity gradient dV/dx at wall ($x = R_2$) of side branch = 97.9 s^{-1}]. (a) Side-branch 1; (b) Side-branch 2.

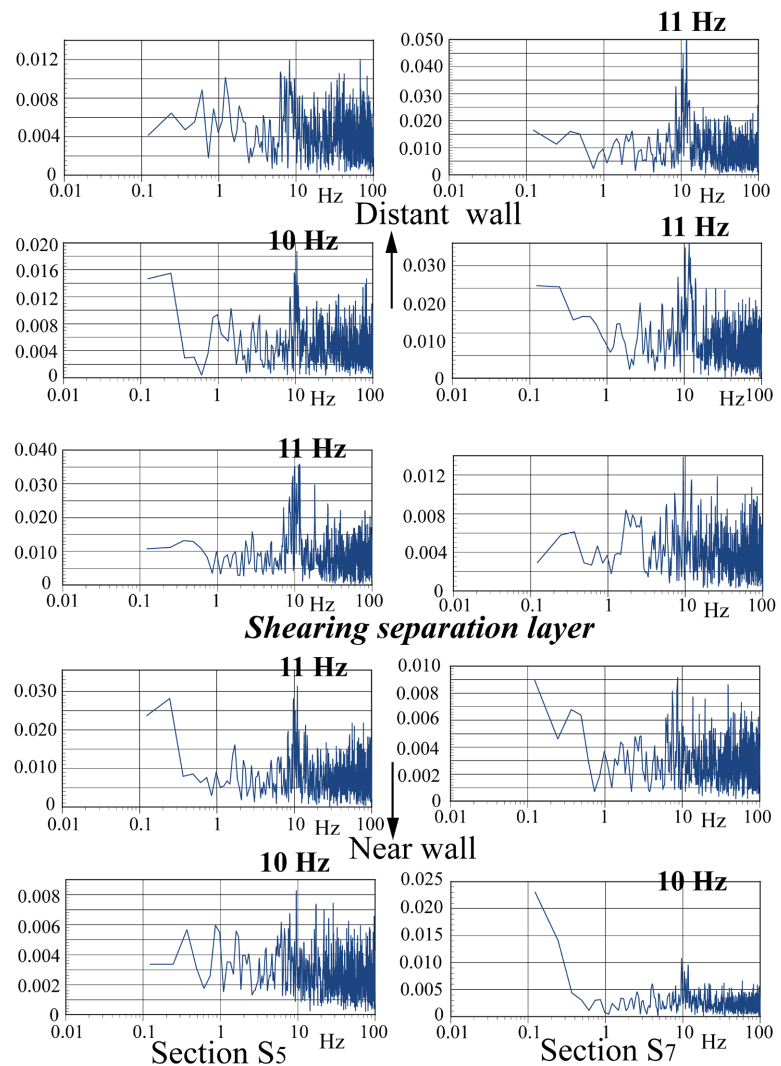


Figure 20. Spectral analysis in branch 2.

2.5. Karman Vortex Downstream of an Island in Ocean in Meteorology

Karman vortices are observed on a huge scale around islands in the ocean. **Figure 3(a)** and **Figure 4** show such a Karman vortex as described in Section 2.1. The Reynolds number of this stream is estimated as follows.

$$Re = L(30 \text{ km}) \times U(50 \text{ m/s}) / \nu(5 \text{ m}^2/\text{s}) = 3 \times 10^5.$$

This order of 10^5 is comparable to that in the field of fluid engineering. In other words, although the field of fluid engineering associates with the Karman vortex with molecular kinematic viscosity, the same feature is seen in meteorology.

3. Prediction of Flow Instability in Fluid Power Plant

Sections 2.2 to 2.5 presented periodic oscillations in single and double side-branches and described how the Strouhal number is independent of the

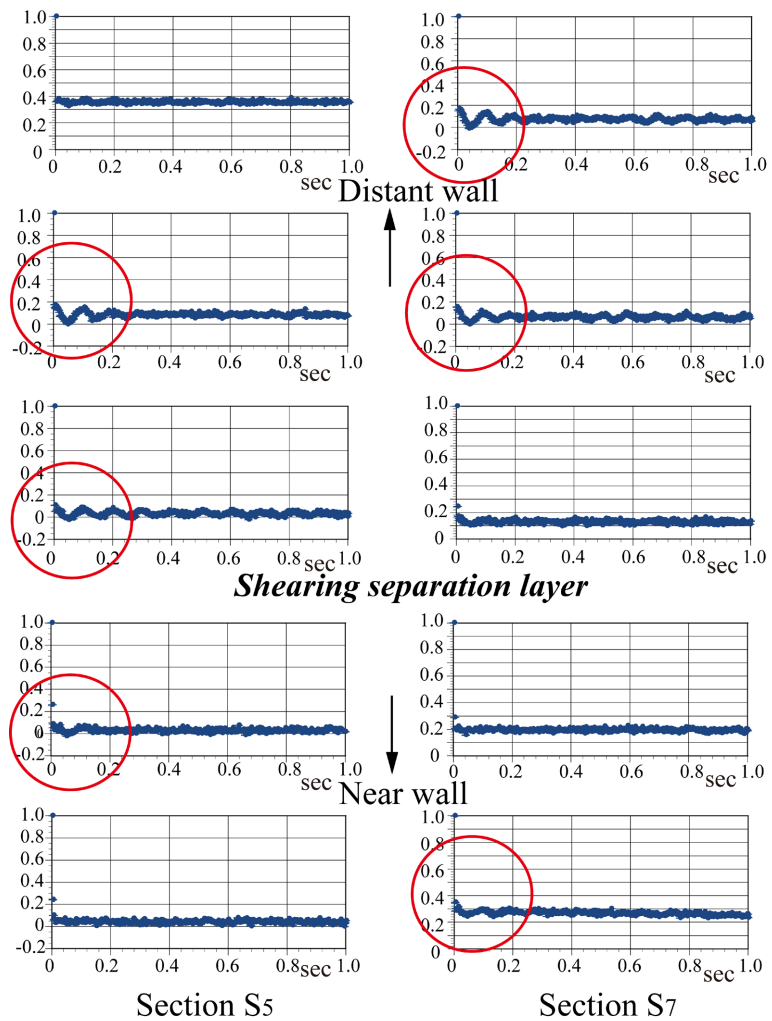


Figure 21. Auto-correlation in branch 2.

Reynolds number, flow division ratio, and ratio of tube radii. This oscillation of flow is basically related to the high-shear-rate flow in a side-branch and the geometry of the inlet of the side-branch; *i.e.*, a square-edged corner. T-junctions with square-edged corners are generally used in the pipeline network of a fluid power plant as shown in **Figure 22**. The connecting corner usually has a sharp square edge because a side-branch in a pipeline network is welded to the trunk at the construction site, as shown in **Figure 23**. There is a slight possibility of induced to be flow instability even in a turbulent flow. Here, we denote this flow instability induced in the side-branch with the high-shear-rate flow, that is, along with the shearing separation layer. The connecting geometry of the trunk and side branch should have rounded corners rather than sharp corners to suppress this high shear rate.

It will be difficult to predict another flow phenomenon from past research, because fluid dynamics phenomena are generally nonlinear. Recently, there have been many unex-incidents at fluid power plants, such as the destruction of a fine heat exchange tube. It will be difficult to predict another flow phenomenon from past researches because fluid dynamics phenomena are generally nonlinear.

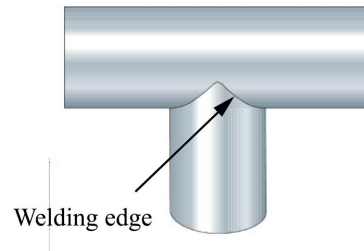


Figure 22. Geometry of T-junction.



Figure 23. Construction site in welding pipeline.

Recently, there have been many unexpected incidents at fluid power plants, such as the destruction of a fine heat exchange tube in the Mihama Nuclear Power Plant in Japan, schematically shown in **Figure 24** [6]. This incident resulted from fluid dynamic vibration accompanying a Karman vortex. Although a major cause of the vibration was the unsuitable installation of the fine steam tube on a supporting plate, the frequency of flow instability based on a Strouhal number $St = 0.2$ [40] is estimated to be $f = USt/d = 5.2 \times 0.2/0.02 = 52$ Hz, where $U = 0.52$ m/s is temporarily assumed to be the mean velocity in the steam generator, $d = 0.02$ m is the diameter of the heat exchanger fine tube, and $Re = Ud/\nu = 5.2 \times 0.02/10^{-6} = 10^5$.

Another incident was the leakage of liquid sodium due to the destruction of a thermocouple in the Monju fast breeder reactor in Japan, schematically shown in **Figure 25**. Neither the designer nor the researcher could predict either incident before construction. In the Monju fast breeder reactor constructed using straight tubes, T-junctions, and elbows, presumably the fluid oscillation based on the current review is tried to estimate the fluid vibration in T-junction. Using data provided by Monju FBR Co. [2], the frequency of oscillation of flow instability in a T-junction can be predicted from the current Strouhal number $St = 1.02$, tube diameter $D = 54$ cm, kinematic viscosity of the working fluid (liquid sodium at a temperature of 400°C) $\nu = 0.3323 \times 10^{-6}$ m²/s, and mean velocity $U = 5.2$ m/s in working operation as [2]

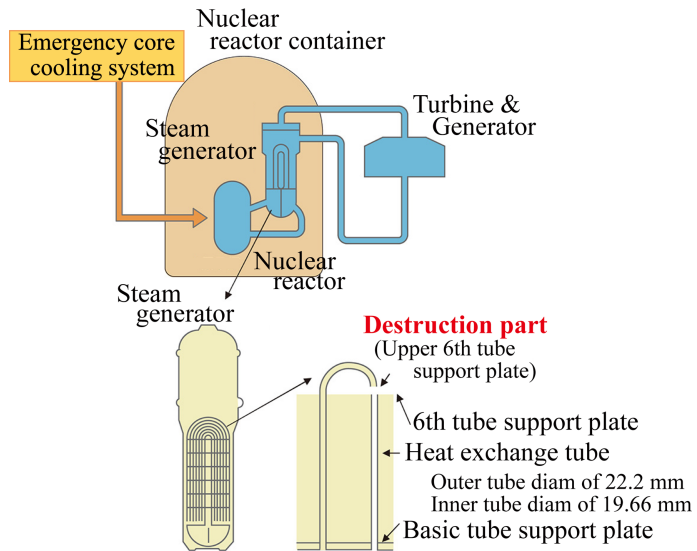


Figure 24. Structure and destruction part of Mihama nuclear power plant.

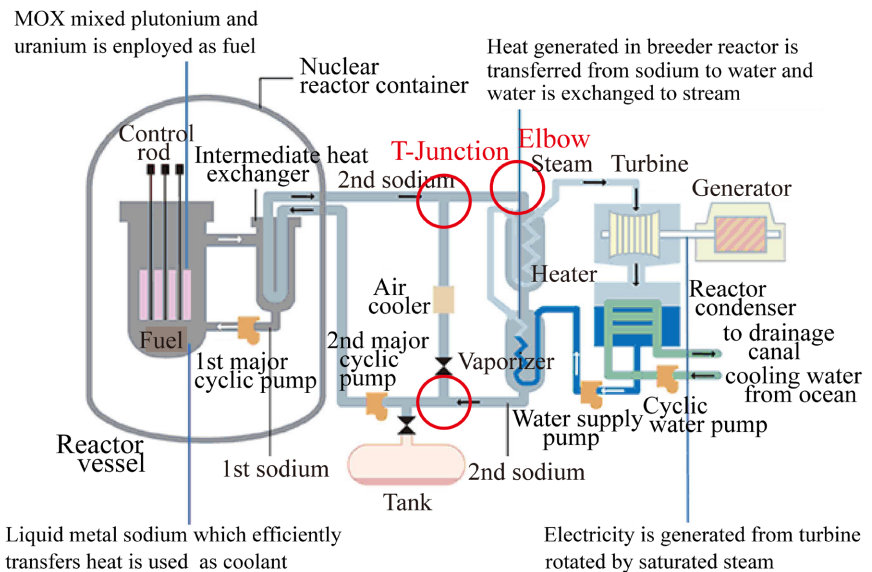


Figure 25. Global schema of fast breeder reactor “MONJU”.

$$f = USt/D = 5.2 \times 1.02 / 0.54 = 9.82 \text{ Hz}$$

The Reynolds number for the side-branch is estimated as

$$Re = DU/\nu = 0.54 \times 5.2 / 0.3323 \times 10^{-6} = 8.45 \times 10^6$$

Meanwhile, the vibration of flow around a thermocouple in the Monju fast breeder reactor has a frequency $f = 52 \text{ Hz}$ at a Strouhal number of 0.2 for a Karman vortex at $Re = 3.3 \times 10^5$.

Including the Karman vortex downstream of the island, the order of the Reynolds number is approximately $10^5 - 10^6$. There is a slight possibility for fluid-induced vibration to occur in this range of the Reynolds number. This possibility should be considered by the designer of a fluid power plant.

Acknowledgements

This review was partially supported by JSPS Science Research Budgets #09450083, #12650180, #144550160 & #19K04163. The authors thank Edanz (<https://jp.edanz.com/ac>) for editing a draft of this manuscript.

Conflicts of Interest

The authors have no conflict of interest.

References

- [1] Benard, H. (1908) Formation périodique de centres de giration à l'arrière d'un obstacle en mouvement. *Comptes Rendus de l'Académie des Sciences Paris*, **147**, 839-842.
- [2] Von Karman, Th. (1911) Über den Mechanismus des Widerstandes, den ein bewegter Körper in einer Flüssigkeit erzeuge. *Nachrichten von der Gesellschaft der Wissenschaften zu Göttingen, Mathematisch-Physikalische Klasse*, **1911**, 509-517.
- [3] Von Karman, Th. and Rubach, H. (1921) Über den Mechanismus, des Flüssigkeits- und Luftwiderstandes. *Physikalische Zeitschrift*, **13**, 49-59.
- [4] Takoma Bridge Incident.
<https://www.google.com/search?q=tacoma+narrows+bridge+collapse>
- [5] Monju Incident 1995. (In Japanese)
<http://www.aec.go.jp/jicst/NC/senmon/old/koso/siryu/koso01/siryu07.htm>
- [6] Mihama Nuclear Power Plant Incident 1991. (In Japanese)
https://atomica.jaea.go.jp/data/detail/dat_detail_02-07-02-04.html
- [7] Brown, G.L. and Roshko, A. (1974) On Density Effects and Large Structure in Turbulence Mixing Layers. *Journal of Fluid Mechanics*, **64**, 775-816.
<https://doi.org/10.1017/S002211207400190X>
- [8] Tani, I. (1964) Low-Speed Flows Involving Bubble Separation. *Progress in Aeronautical Sciences*, **5**, 79-103. [https://doi.org/10.1016/0376-0421\(64\)90004-1](https://doi.org/10.1016/0376-0421(64)90004-1)
- [9] Taneda, S. (1963) The Stability of Two-Dimensional Laminar Wakes at Low Reynolds Number. *Journal of the Physical Society of Japan*, **18**, 288-296.
<https://doi.org/10.1143/JPSJ.18.288>
- [10] Sarohia, V. (1977) Experimental Investigation of Oscillations Flows over Shallow Cavities. *AIAA Journal*, **15**, 984-991. <https://doi.org/10.2514/3.60739>
- [11] Rockwell, D. and Naudascher, E. (1978) Review-Self-Sustaining Oscillations of Flow past Cavities. *ASME Journal of Fluids Engineering*, **100**, 152-165.
<https://doi.org/10.1115/1.3448624>
- [12] Sherwin, S.J. and Blackburn, H.M. (2005) Three-Dimensional Instabilities and Transition of Steady and Pulsatile Axisymmetric Stenotic Flows. *Journal of Fluid Mechanics*, **533**, 297-327. <https://doi.org/10.1017/S0022112005004271>
- [13] Mori, T. and Nagamura, K. (2010) LDV and PIV Measurements of the Organized Oscillations of Turbulent Flow over a Rectangular Cavity. *Journal of Fluid Science and Technology*, **5**, 370-383. <https://doi.org/10.1299/jfst.5.370>
- [14] Baes, A.J., Dooly, D.J., Schroter, R.C., Cetto, R., Calmet, H., Gambaruto, A.M., Tolly, N. and Houzeaux, G. (2015) Dynamics of Airflow in a Short Inhalation. *Journal of the Royal Society Interface*, **12**, Article ID: 20140880.
<https://doi.org/10.1098/rsif.2014.0880>

- [15] Dooly, D., Taylor, D.J., Franke, P. and Schroter, R.C. (2008) Experimental Investigation of Nasal Airflow. *Journal of Engineering in Medicine*, **222**, 439-453. <https://doi.org/10.1243/09544119JEIM330>
- [16] Balint, T.S. and Lucey, A.D. (2005) Instability of a Cantilevered Flexible Plate in Viscous Channel Flow. *Journal of Fluids and Structures*, **20**, 893-912. <https://doi.org/10.1016/j.jfluidstructs.2005.05.005>
- [17] Keshtkar, H. and Jafari, A.A. (2017) Vibration Analysis of a Turbulent Fluid Passing Inside an Elbow Shaped Pipe Section. *Journal of Applied Mechanical Engineering*, **6**, 273. <https://doi.org/10.4172/2168-9873.1000273>
- [18] Yagi, T., Sato, A., Shinke, M., Takahashi, S., Tobe, Y., Takao, H., Murayama, Y. and Umezu, M. (2013) Experimental Insights into Flow Impingement in Cerebral Aneurysm by Stereoscopic Particle Image Velocimetry: Transition from a Laminar Regime. *Journal of the Royal Society Interface*, **10**, Article ID: 20121031. <https://doi.org/10.1098/rsif.2012.1031>
- [19] Valen-Sendstad, K., Mardal, K.-A., Mortensen, M., Reif, B.A.P. and Langtangen, H.P. (2011) Direct Numerical Simulation of Transitional Flow in a Patient-Specific Intracranial Aneurysm. *Journal of Biomechanics*, **44**, 2826-2832. <https://doi.org/10.1016/j.jbiomech.2011.08.015>
- [20] Valen-Sendstad, K., Mardal, K.-A. and Steinman, D.A. (2013) High-Resolution CFD Detects High-Frequency Velocity Fluctuations in Bifurcation, But Not Side-wall Aneurysms. *Journal of Biomechanics*, **46**, 402-407. <https://doi.org/10.1016/j.jbiomech.2012.10.042>
- [21] Valen-Sendstad, K., Piccinelli, M. and Steinman, D.A. (2014) High-Resolution Computational Fluid Dynamics Detects Flow Instabilities in the Carotid Siphon: Implications for Aneurysm Initiation and Rupture? *Journal of Biomechanics*, **47**, 3210-3216. <https://doi.org/10.1016/j.jbiomech.2014.04.018>
- [22] Il'ichev, A.T. and Fu, Y.-B. (2012) Stability of Aneurysm Solutions in a Fluid-Filled Elastic Membrane Tube. *Acta Mechanica Sinica*, **28**, 1209-1218. <https://doi.org/10.1007/s10409-012-0135-2>
- [23] Baek, H., Jayaraman, M.V., Richardson, P.D. and Karniadakis, G.E. (2010) Flow Instability and Wall Shear Stress Variation in Intracranial Aneurysms. *Journal of the Royal Society Interface*, **7**, 967-988. <https://doi.org/10.1098/rsif.2009.0476>
- [24] Awasthi, M.K. (2013) Nonlinear Analysis of Rayleigh-Taylor Instability of Cylindrical Flow with Heat and Mass Transfer. *Journal of Fluids Engineering-Transactions of the ASME*, **135**, Article ID: 061205. <https://doi.org/10.1115/1.4024001>
- [25] Bernard, T., Truman, C.R., Vorobieff, P., Corbin, C., Wayne, P.J., Kuehner, G. and Anderson, M. and Kumar, S. (2015) Observation of the Development of Secondary Features in a Richtmyer-Meshkov Instability Driven Flow. *Journal of Fluids Engineering-Transactions of the ASME*, **137**, Article ID: 011206. <https://doi.org/10.1115/1.4027829>
- [26] Liu, L.J. and Lu, L.P. (2014) Instability of Viscoelastic Annular Liquid Jets in a Radial Electric Field. *Journal of Fluids Engineering*, **136**, Article ID: 081202. <https://doi.org/10.1115/1.4026925>
- [27] Bouzgarrou, G., Bury, Y., Jamme, S., Joly, L. and Haas, J.F. (2014) Laser Doppler Velocimetry Measurements in Turbulent Gaseous Mixing Induced by the Richtmyer-Meshkov Instability: Statistical Convergence Issues and Turbulence Quantification. *Journal of Fluids Engineering*, **136**, Article ID: 091209. <https://doi.org/10.1115/1.4027311>

- [28] File: Jeju Do von Karman Vortex Street Mar 2 2011 02 35(UTC).
<http://commons.wikimedia.org>
- [29] The Japan Society of Mechanical Engineers (1979) JSME Data Handbook: Hydraulic Losses in Pipes and Ducts. The Japan Society of Mechanical Engineers, Tokyo, 86-95. (In Japanese)
- [30] Karino, T., Kwong, H.H.M. and Goldsmith, H.L. (1979) Particle Flow Behavior in Models of Branching Vessels: I Vortices in 90° T-Junctions. *Biorheology*, **16**, 231-248. <https://doi.org/10.3233/BIR-1979-16312>
- [31] Liepsch, D., Poll, A., Strigberger, J., Sabbah, H.N. and Stein, P.D. (1989) Flow Visualization Studies in a Mold of the Normal Human Aorta and Renal Arteries. *ASME Journal of Biomechanical Engineering*, **111**, 222-227.
<https://doi.org/10.1115/1.3168369>
- [32] Perktold, K. and Peter, R. (1990) Numerical 3D-Simulation of Pulsatile Wall Shear Stress in an Arterial T-Bifurcation Model. *Journal of Biomedical Engineering*, **12**, 2-12. [https://doi.org/10.1016/0141-5425\(90\)90107-X](https://doi.org/10.1016/0141-5425(90)90107-X)
- [33] Yung, C.N., De Witt, K.J. and Keith Jr., T.G. (1990) Three-Dimensional Steady Flow through a Bifurcation. *Journal of Biomechanical Engineering—Transactions of the ASME*, **112**, 189-197. <https://doi.org/10.1115/1.2891171>
- [34] Yamaguchi, R., Mashima, T. and Takahashi, Y. (1997) Separated Secondary Flow and Wall Shear Stress in Side Branch of Right Angle Branch. ASME Paper No. 3303.
- [35] Yamaguchi, R., Shigeta, M., Kudo, S. and Hayase, T. (2000) Wall Shear Stress and Periodical Oscillation Induced in Side Branch at Right Angle Branch in Laminar Steady Flow. ASME Paper No. 11085.
- [36] Tanaka, G., Yamaguchi, R., Liu, H. and Hayase, T. (2016) Fluid Vibration Induced by High-Shear-Rate Flow in a T-Junction. *ASME Journal of Fluids Engineering*, **138**, Article ID: 081103. <https://doi.org/10.1115/1.4032935>
- [37] Yamaguchi, R., Tanaka, G., Liu, H. and Hayase, T. (2016) Fluid Vibration Induced in T-Junction with Double Side Branches. *WJM*, **6**, 169-179.
<https://doi.org/10.4236/wjm.2016.64014>
- [38] Yamaguchi, R., Tanaka, G., Liu, H. and Hayase, T. (2017) Universality of Periodic Oscillation Induced in Side Branch of a T-Junction in Numerical Simulation. *Journal of Flow Control, Measurement & Visualization*, **5**, 73-85.
<http://www.scirp.org/journal/jfcmv>
- [39] Yamaguchi, R., Mashima, T., Amagai, H., Fujii, H., Hayase, T. and Tanishita, K. (2005) Variation of Wall Shear Stress and Periodic Oscillations Induced in the Right-Angle Branch during Laminar Steady Flow. *ASME Journal of Fluids Engineering*, **127**, 1013-1020. <https://doi.org/10.1115/1.1852480>
- [40] Schlichting, H. (1976) Boundary Layer Theory. 7th Edition, McGraw-Hill Book, New York, 32.

Nomenclature

f	frequency of fluid vibration
n	ordinate normal to the separation shearing layer
Q_s	rate of flow through the side-branch
Q_T	rate of flow through the trunk
q	tangential velocity along the shearing separation layer
$Re_s = 2R_s U_s / \nu$	Reynolds number based on variables of the side-branch
$Re_T = 2R_T U_T / \nu$	Reynolds number based on variables of the trunk
R_s	radius of the side-branch
R_T	radius of the trunk
$St_s = 2fR_s / U_s$	Strouhal number based on variables of the side-branch
U_s	mean velocity in the side-branch
U_T	mean velocity in the trunk
u	transverse velocity in the side-branch
v	axial velocity in the side-branch
ρ	density of the fluid
ν	molecular kinematic viscosity of the fluid
ε	eddy kinematic viscosity